# Studies on the mechanism of general anesthesia

Mahmud Arif Pavel[a,b], E. Nicholas Petersen[a,b], Hao Wang[a,b], Richard A. Lerner[c,1], and Scott B. Hansen[a,b,1]

[a]Department of Molecular Medicine, The Scripps Research Institute, Jupiter, FL 33458; [b]Department of Neuroscience, The Scripps Research Institute, Jupiter, FL 33458; and [c]Department of Chemistry, The Scripps Research Institute, La Jolla, CA 92037

**Inhaled anesthetics are a chemically diverse collection of hydrophobic molecules that robustly activate TWIK-related K$^+$ channels (TREK-1) and reversibly induce loss of consciousness. For 100 y, anesthetics were speculated to target cellular membranes, yet no plausible mechanism emerged to explain a membrane effect on ion channels. Here we show that inhaled anesthetics (chloroform and isoflurane) activate TREK-1 through disruption of phospholipase D2 (PLD2) localization to lipid rafts and subsequent production of signaling lipid phosphatidic acid (PA). Catalytically dead PLD2 robustly blocks anesthetic TREK-1 currents in whole-cell patch-clamp recordings. Localization of PLD2 renders the TRAAK channel sensitive, a channel that is otherwise anesthetic insensitive. General anesthetics, such as chloroform, isoflurane, diethyl ether, xenon, and propofol, disrupt lipid rafts and activate PLD2. In the whole brain of flies, anesthesia disrupts rafts and PLD$^{null}$ flies resist anesthesia. Our results establish a membrane-mediated target of inhaled anesthesia and suggest PA helps set thresholds of anesthetic sensitivity in vivo.**

lipid raft | phospholipase D | potassium channel | consciousness | substrate presentation

In 1846 William Morton demonstrated general anesthesia with inhaled anesthetic diethyl ether (1). For many anesthetics (but not all), lipophilicity is the single most significant indicator of potency; this observation is known as the Meyer–Overton correlation (2, 3). This correlation, named for its discoverers in the late 1800s, and the chemical diversity of anesthetics (*SI Appendix*, Fig. S1*A*) drove anesthetic research to focus on perturbations to membranes as a primary mediator of inhaled anesthesia (3). Over the last two decades, enantiomer selectivity of anesthetics suggested a chiral target, and direct binding to ion channels emerged (4). But the possibility of a membrane-mediated effect has remained (5–7).

Within the membrane, regions of ordered lipids, sometimes called lipid rafts, allow for nanoscale compartmentalization of proteins and lipids (8). The best-studied lipid rafts are comprised of cholesterol and saturated lipids including sphingomyelin (e.g., monosialotetrahexosylganglioside1 [GM1]) (*SI Appendix*, Fig. S1 *B* and *C*) (9, 10) and bind cholera toxin B (CTxB) with high affinity (8). Their exact size in vivo is still debated (11–14), but in cultured cells with high cholesterol, a condition most relevant to the high cholesterol in brain (~45% off total lipids) (15), they are ~100 nm in diameter (16).

Anesthetics are speculated to disrupt lipid rafts. An early theory suggested that anesthetic disruption of crystallin lipids surrounding a channel (i.e., rafts) could directly activate the channel by changing its lipid environment (17). Consistent with this theory, anesthetics lower the melting temperature and expand the apparent size of GM1 rafts (18–20), and GM1 rafts influence ion channels (21). However, direct experimental evidence linking these biophysical properties to an ion channel in the membrane or any other anesthetic-sensitive protein is lacking.

We recently showed that mechanical force disrupts lipid rafts and that the disruption activates the enzyme phospholipase D2 (PLD2) (22). PLD2 is palmitoylated at cysteines near its Pleckstrin homology (PH) domain, which is required to localize it to GM1

lipid rafts (GM1 rafts) (23, 24). The PH domain also binds phosphatidylinositol 4,5-bisphosphate (PIP$_2$) which opposes localization by palmitoylation (*SI Appendix*, Fig. S1*C*). PIP$_2$ is polyunsaturated and forms its own domains separate (~42 nm) from GM1 rafts (22, 25, 26). PIP$_2$ rafts are cholesterol independent and colocalize with PLD2 substrate phosphatidylcholine (PC) (*SI Appendix*, Fig. S1 *B* and *C*) (22). PLD2's translocation to PIP$_2$ rafts facilitates PC hydrolysis and the production of phosphatidic acid (PA) (*SI Appendix*, Fig. S1*C*) (22, 27, 28).

TREK-1 is an anesthetic-sensitive two-pore-domain potassium (K2P) channel that is activated by PLD2 (29). PLD2 activates TREK-1 by binding to a disordered C terminus and producing high local concentrations of PA that activate the channel—the PLD1 isoenzyme does not activate the channel (29). Inhaled anesthetics xenon, diethyl ether, halothane, and chloroform robustly activate TREK-1 at concentrations relevant to their clinical use (30, 31). Genetic deletion of TREK-1 decreases anesthesia sensitivity in mice (32), establishing the channel as a relevant target of anesthetics in vivo.

We hypothesized anesthetics could activate TREK-1 indirectly by disruption of lipid rafts. If correct, this would constitute a mechanism distinct from the usual receptor–ligand interaction and establish a definitive membrane-mediated mechanism for inhaled anesthesia. Here we show that anesthetics disrupt GM1 rafts and activate TREK-1 through a two-step PLD2-dependent mechanism.

## Significance

**Anesthetics are used every day in thousands of hospitals to induce loss of consciousness, yet scientists and the doctors who administer these compounds lack a molecular understanding for their action. The chemical properties of anesthetics suggest that they could target the plasma membrane. Here the authors show anesthetics directly target a subset of plasma membrane lipids to activate an ion channel in a two-step mechanism. Applying the mechanism, the authors mutate a fruit fly to be less sensitive to anesthetics and convert a nonanesthetic-sensitive channel into a sensitive one. These findings suggest a membrane-mediated mechanism will be an important consideration for other proteins of which direct binding of anesthetic has yet to explain conserved sensitivity to chemically diverse anesthetics.**

NEUROSCIENCE

**Anesthetic Perturbations to Lipid Rafts.** To establish an anesthetic effect on GM1 rafts in cellular membrane, we treated neuroblastoma 2A (N2A) cells with anesthetic chloroform at 1 mM concentration and monitored fluorescent CTxB clustering by direct stochastical optical reconstruction microscopy (dSTORM) (Fig. 1A). GM1 rafts are below the diffraction limit of light and require super-resolution imaging like dSTORM for their characterization.

Fig. 1 B and C shows chloroform strongly increased both the apparent diameter and area of GM1 rafts in the cell membrane (Fig. 1 B and C and *SI Appendix*, Fig. S2A). The apparent diameter is the observed diameter at a given cluster radius. Isoflurane (1 mM) behaved similarly to chloroform (Fig. 1 A–C). The Ripley's radius, a measure of the apparent space between domains, decreased dramatically for both chloroform and isoflurane (*SI Appendix*, Fig. S2B). Furthermore, both number of rafts and total area per cell increased (Fig. 1 D–F and *SI Appendix*, Fig. S2C).

Methyl-β-cyclodextrin (MβCD), a chemical that removes cholesterol from the membrane and disrupts GM1 lipid rafts (22), reduced the total number of GM1 rafts (Fig. 1D). Binning the rafts into small (0 to 150 nm) and large (150 to 500 nm) apparent diameters revealed a clear shift from small to large

rafts in the presence of inhaled anesthetics and revealed the opposite effect after MβCD treatment (*SI Appendix*, Fig. S2D). Similar results were obtained in C2C12 myoblasts (muscle cells); chloroform strongly increased both the apparent diameter and area of GM1 rafts (*SI Appendix*, Fig. S2 E–H).

**Mechanism of Anesthetic Sensitivity in TREK-1 Channels.** Activation of TREK-1 by inhaled anesthetics, was previously shown to require a disordered loop in the channel's C terminus (30) (*SI Appendix*, Fig. S3 A and B). PLD2 also binds to and activates through the same C-terminal region in TREK-1 (29). We hypothesized, if the anesthetic sensitivity is through PLD2, then blocking PLD2's catalytic activity should block the effects of anesthetics on the channel.

To directly test the role of PLD2 in TREK-1 activation by anesthetics, we overexpressed TREK-1 with a catalytically dead K758R PLD2 mutant (xPLD2) that blocks PA production (33) in HEK293 cells. We found xPLD2, expressed >10-fold compared to endogenous protein (*SI Appendix*, Fig. S3D), blocked all detectable chloroform-specific current (Fig. 2 A–C). Cells not transfected with TREK-1 had no observable current and were unaffected by chloroform treatment (*SI Appendix*, Fig. S3C), strongly suggesting anesthetic activates TREK-1 channels in
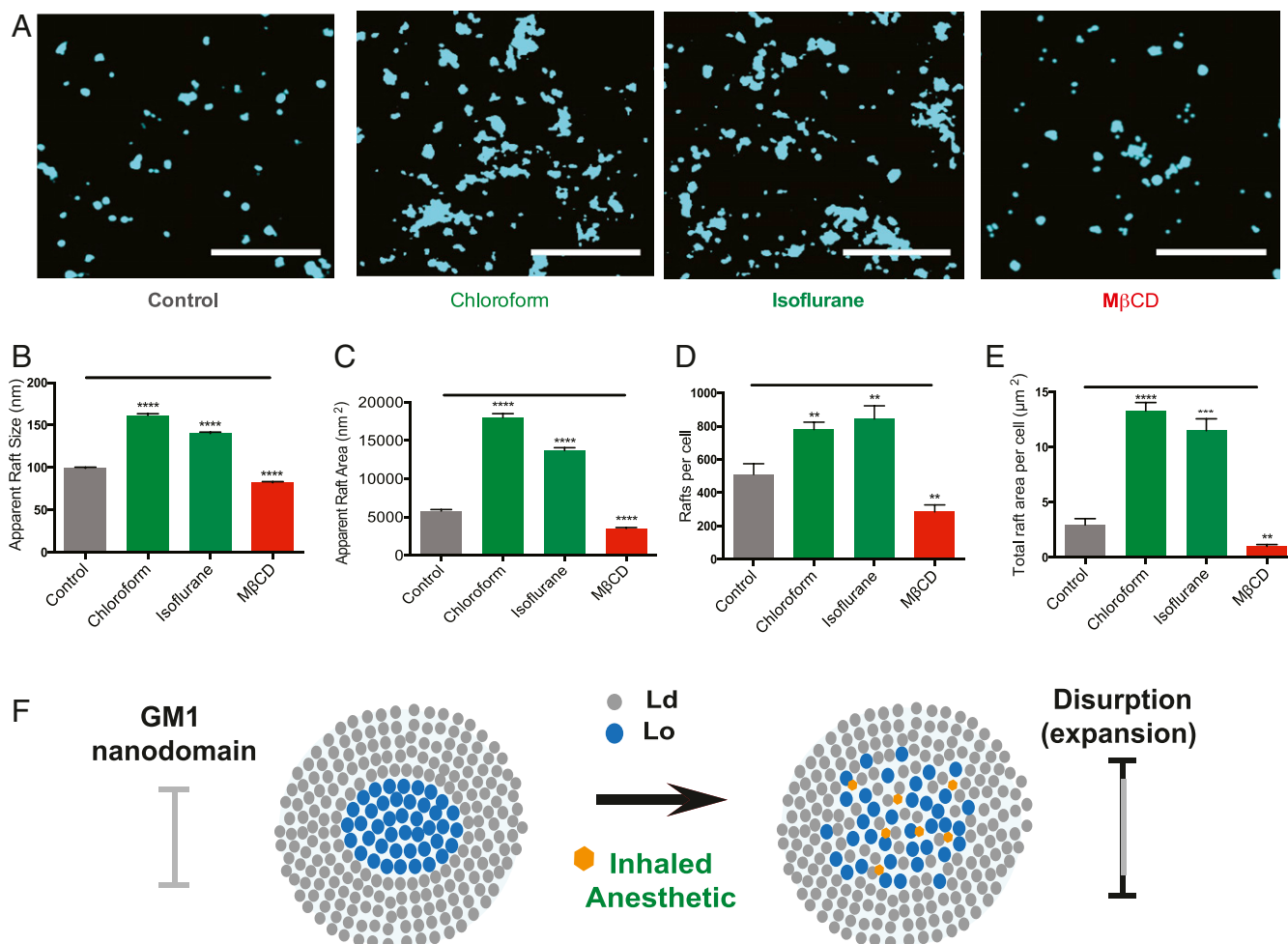


**Fig. 1.** Inhaled anesthetics disrupt GM1 domain's apparent structure. (A) Representative reconstructed super-resolution (dSTORM) images of GM1 rafts before and after treatment with chloroform (1 mM), isoflurane (1 mM), or MβCD (100 μM). (Scale bars, 1 μm.) (B and C) Bar graphs comparing the apparent raft sizes (B) and areas (C) quantified by cluster analysis (±SEM, n = 2,842 to 7,382). (D and E) Quantified number of rafts per cell (D) and total area of rafts per cell (E) (±SEM, n = 10) (Student's t test results: **P < 0.01; ***P < 0.001; ****P < 0.0001). (F) Model representation of raft disruption by anesthetics. GM1 lipids (blue) form lipid rafts. Inhaled anesthetic (orange hexagon) intercalate and disrupt lipid order causing the domain to expand.
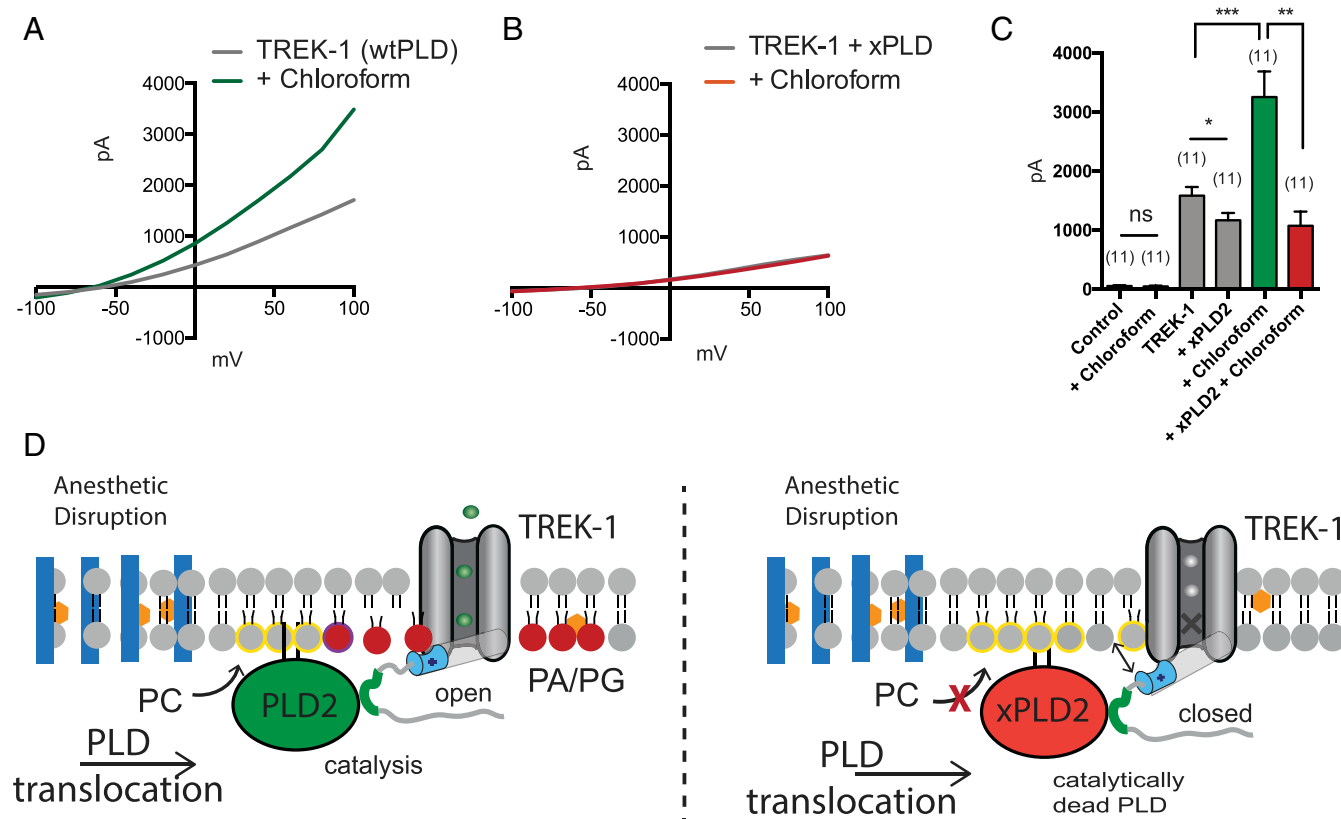
**Fig. 2.** Activation of TREK-1 by inhaled anesthetic is PLD2 dependent. (*A*) Representative TREK-1 whole-cell currents activated by chloroform (1 mM) in physiological K⁺ gradients. The current–voltage relationships (I–V curves) were elicited by 1-s depolarizing pulses from −100 to 100 mV in +20-mV increments. (*B*) Representative I–V curves showing that coexpression of a catalytically inactive mutant of PLD2 (xPLD2 = PLD2_K758R) abolishes the TREK-1 activation by chloroform. (*C*) Bar graph showing the approximately twofold increase of TREK-1 current when activated by chloroform (1 mM) (*n* = 11) at +40 mV (±SEM). (*D*) Schematic representation of TREK-1 activation by inhaled anesthetics (orange hexagon). Anesthetic disruption of GM1 rafts (blue rectangles) causes PLD2 to localize with TREK-1 and its substrate phosphatidylcholine (PC, yellow circle) in the disordered region of the membrane. As PLD2 hydrolyzes PC to phosphatidic acid (PA, red sphere), the anionic lipid binds to a known gating helix (gray cylinder), with a lipid binding site (cyan) (36), that activates TREK-1. Student's *t* test results: *$P < 0.05$; **$P < 0.01$; ***$P < 0.001$; ns ≥ $P$ 0.05.

cultured cells almost entirely through a PLD2-dependent process (Fig. 2*D*). The channel failed to open in the absence of PLD2 despite very high concentrations of anesthetics in a biological membrane.

**Transfer of Anesthetic Sensitivity to TRAAK Channel.** TWIK-related arachidonic acid-stimulated K⁺ channel (TRAAK) is an anesthetic-insensitive homolog of TREK-1 (*SI Appendix*, Fig. S3*E*). Interestingly, native TRAAK is also insensitive to PLD2 (29). However, concatenating PLD2 to the N terminus maximally activates TRAAK and introduction of the PLD2 binding domain from TREK-1 renders TRAAK PLD2 sensitive (29). If PLD2 is responsible for anesthetic sensitivity in TREK-1, we reasoned we could render TRAAK anesthetic sensitive by introducing the PLD2 binding site into the C terminus of TRAAK (Fig. 3*A*).

We overexpressed the previously characterized PLD2-sensitive TRAAK chimera (29) (TRAAK/ctTREK) in HEK cells. As expected, in the presence of 1 mM chloroform, TRAAK/ctTREK robustly responded to chloroform (Fig. 3 *B–D*). To confirm the response is due to PLD2 localization and not a direct interaction of the anesthetic with a structural feature of the TREK-1 C terminus, we overexpressed the chimera with xPLD2 and found chloroform had no effect on the channel.

Since the transmembrane domain was identical in TRAAK and TRAAK/ctTREK, this result suggests that the transmembrane domain is not the site of anesthetic sensitivity in

TREK-1 channels; rather, PLD2 and the production of PA imbue the channel with anesthetic sensitivity (Fig. 3*E*). Furthermore, the lack of TREK-1 current in the presence of anesthetic (Fig. 2 *B* and *C*) suggests direct binding of anesthetic is insufficient to activate the channel. This result appears to contradict what was previously thought, that the anesthetic is capable of directly activating TREK-1 (34).

To further test if anesthetics can directly activate TREK-1, we reconstitute purified TREK-1 into lipid vesicles and tested ion flux with and without anesthetic in a cell-free system (35–37). Efflux of potassium was coupled to proton acidification of the vesicles and a fluorometric readout of pH (see *Materials and Methods, Channel Purification and Flux Assay*).

Functionally reconstituted TREK-1 (from zebrafish) in 16:1 PC liposomes with 18:1 phosphatidylglycerol (PG) (85:15 mol% ratio) was unaffected by chloroform or isoflurane (1 mM) (*SI Appendix*, Fig. S3 *F* and *G*). To assure that the channel was properly reconstituted and in conditions capable of increased potassium flux, we reconstituted a mutant TREK-1 with double cysteines that covalently locks TREK-1 in the activated state (36, 38). In a previous study, the same assay showed a clear direct inhibition with local anesthetics (37) further demonstrating TREK-1 is functionally reconstituted in our purified assay. Yet, compared to the open TREK-1 control, inhaled anesthetics failed to activate TREK-1 (*SI Appendix*, Fig. S3 *F* and *G*).
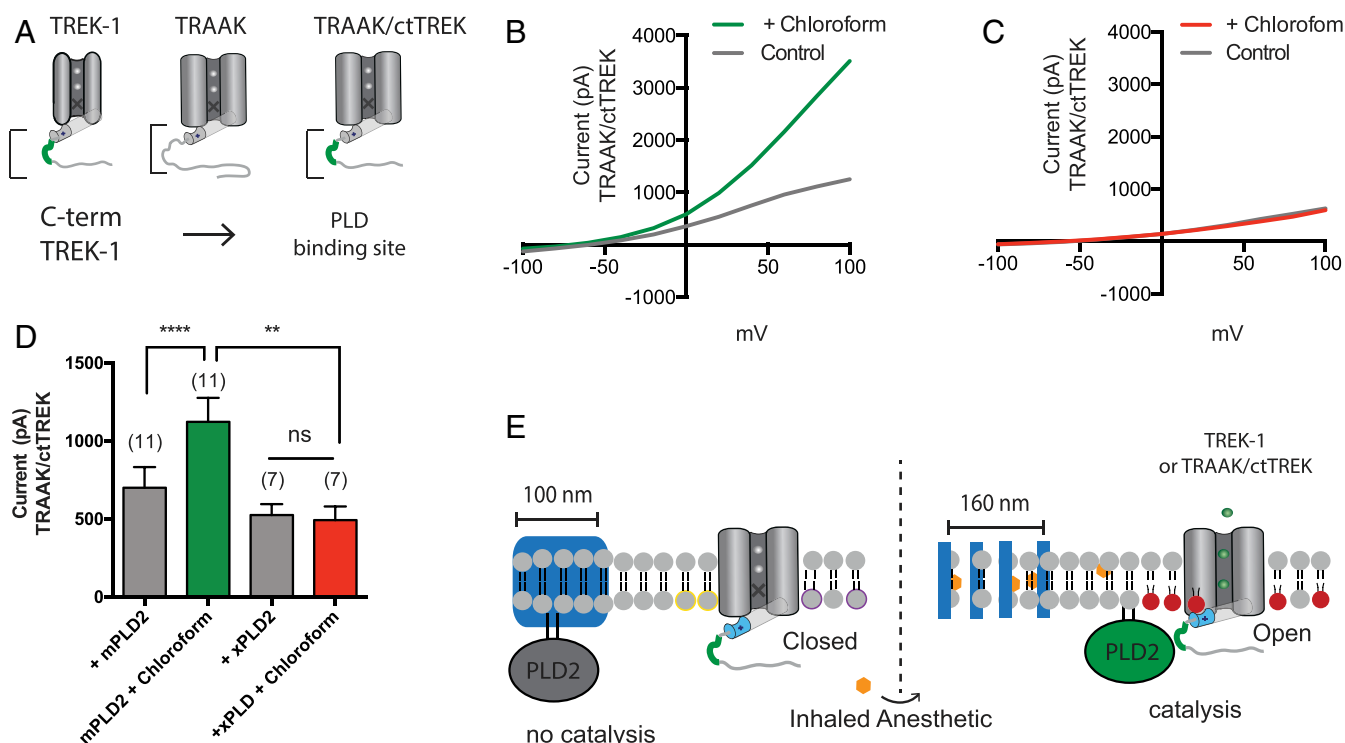
**Fig. 3.** PLD2 localization renders TRAAK anesthetic sensitive. Native TRAAK is an anesthetic-insensitive channel. (*A*) Cartoon showing the experimental setup. TRAAK is fused with the C terminus of TREK-1 (TRAAK/ctTREK). The PLD2 binding site is depicted in green. (*B* and *C*) Representative I–V curve showing TRAAK/ctTREK-1 is activated by chloroform when coexpressed with mouse PLD2 (mPLD2) (*B*). The coexpression of the catalytically inactive PLD2 (xPLD2) abolishes the chloroform activation of TRAAK/ctTREK-1 chimeric channel (±SEM, n = 7) (*C*). (*D*) Bar graph summarizing TRAAK/ctTREK-1 chimeric channel current in the presence or absence of xPLD2 and chloroform (1 mM) at +40 mV (±SEM, n = 11) (Student's *t* test results: ns P > 0.05; **P ≤ 0.01; ****P ≤ 0.0001). (*E*) Model mechanism showing that anesthetics activate the TRAAKctTREK-1 chimeric channel through raft disruption and PLD2 substrate presentation; xPLD2 abolishes the activation (the color scheme is as in Fig. 2).

## Anesthetics Disruption of PLD2 Localization to Lipid Rafts.

We reasoned that if anesthetics activate PLD2 then we should see a translocation of PLD2 away from GM1 rafts. To directly monitor translocation of PLD2, we imaged colocalization of PLD2 with GM1 rafts using dSTORM. Translocation was determined by calculating a pairwise correlation of PLD2 with CTxB-labeled lipids before and after anesthetic treatment. Pairwise correlation avoids potential artifacts from oversampling and user-selected parameters used when determining apparent raft size (*SI Appendix*, Fig. S4) (27). Both N2A and C2C12 endogenously express TREK-1 and PLD2 (*Materials and Methods*) allowing us to characterize their translocation under endogenous promoters. TREK-1 is not palmitoylated, but the protein is complexed with PLD2, which is palmitoylated (29), and sequesters the prebound PLD2/TREK-1 complex into GM1 domains away from PLD's substrate (PC) (22) (*SI Appendix*, Fig. S1 *B* and *C*).

Treating the N2A cells with chloroform or isoflurane (1 mM), caused PLD2 to translocate away from GM1 lipids (Fig. 4*A*). Pair correlation analysis showed PLD2 strongly associated with GM1 rafts prior to anesthetic treatment (Fig. 4*B*, gray trace) but only weakly associated after treatment (green traces). This highly significant anesthetic-induced change in PLD2 localization was true across all sizes of GM1 rafts (Fig. 4 *B* and *C*, pair correlation analysis), suggesting the energetics of PLD2 partitioning into GM1 lipids changed, not merely a change in the apparent size of the raft. The anesthetic-specific translocation was similar in magnitude to MβCD-stimulated translocation of PLD2 (Fig. 2 *B* and *C*) and implies that disruption by removing cholesterol and disruption by anesthetics has the same effect on PLD2 localization to lipid rafts (Fig. 4*D*). We obtained similar pair correlation

results in C2C12 cells treated with chloroform (*SI Appendix*, Fig. S5 *B* and *C*).

CTxB is a pentadentate toxin that can cause nanoscale clustering in live and fixed cells (16, 27). Since CTxB-induced clustering of GM1 lipids would sequester PLD2, not release it, it is unlikely that CTXB-induced artificial clustering accounts for PLD2 translocation. Nonetheless, we tested mobility of lipids in our fixed membranes (e.g., mobility between GM1 and PIP2 rafts) using fluorescence recovery after photobleaching (FRAP). FRAP showed minimal mobility of CTxB-bound lipids after fixing in C2C12 cells (*SI Appendix*, Fig. S5*E*). Furthermore, fixed PLD2 was about the same apparent size as GM1 rafts in both N2A and C2C12 cells as expected (*SI Appendix*, Fig. S5*E*) (27).

## Anesthetic Activation of PLD.

If the membrane is a general mechanism for TREK-1-mediated anesthesia, then most known activators of TREK-1 should also activate PLD2. We tested enzymatic activation of PLD by treating live cells with a spectrum of chemically diverse inhaled anesthetics and monitoring activity using an assay that couples PLD's choline release (both iso-enzyme 1 and 2) to a fluorescent signal (22) (Fig. 5*A*). Diethyl ether, chloroform, isoflurane, and xenon all significantly activated PLD2 in N2A (Fig. 5*B* and *SI Appendix*, Fig. S6*A*) and C2C12 cells (*SI Appendix*, Fig. S6 *B* and *C*). Isoflurane had the greatest effect (Fig. 5*B*) in N2A cells and chloroform had the greatest effect in C2C12 cells (*SI Appendix*, Fig. S6 *A* and *B*). The dose–response of chloroform and isoflurane reveals a half maximal effective concentration $EC_{50}$ of $1.0 \pm 0.56$ mM and $0.8 \pm$ mM, respectively (Fig. 5 *C* and *D*) in N2A cells. The Hill slopes were $2.4 \pm 2.8$ and $1.3 \pm 0.89$, respectively. Ketamine, an
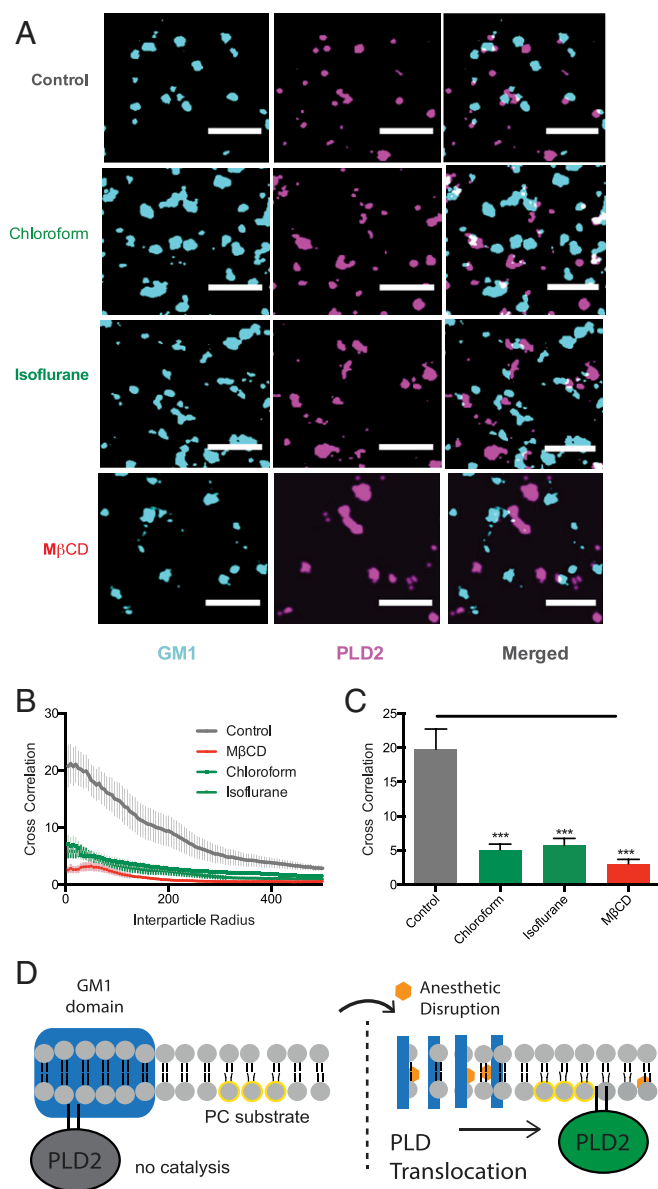
Pavel et al.

**Fig. 4.** Inhaled anesthetics displace PLD2 from GM1 rafts. (*A*) Representative super-resolution (dSTORM) images of fluorescently labeled CTxB (lipid raft) and PLD2 before treatment (control) and after treatment with chloroform (1 mM), isoflurane (1 mM), and MβCD (100 μM) in N2A cells (Scale bars, 0.5 μm.) (*B*) Average cross-correlation functions [C(r)] showing a decrease in PLD2 association with ordered GM1 rafts after treatment with anesthetic or MβCD. (*C*) Comparison of the first data point in *B* (5-nm radius) (±SEM, n = 10 to 17) (Student's *t* test results: ***$P \leq 0.001$). (*D*) Schematic representation of PLD2 in GM1 rafts before (*Left*) and after (*Right*) anesthetic treatment. Palmitoylation drives PLD2 into GM1 rafts (blue rectangle) away from its unsaturated PC substrate (yellow circle). Anesthetics (orange hexagon) disrupts GM1 rafts causing the enzyme to translocate where it finds its substrate PC in the disordered region of the cell.

injectable *N*-methyl-D-aspartate receptor-specific anesthetic (39) and F6, a nonimmobilizer that defies the Meyer–Overton rule, had no effect on PLD activity, as expected (Fig. 5 *A* and *B*).

We also tested the injectable general anesthetics propofol (50 μM) (4). Propofol robustly activated PLD2 in N2A cells (Fig. 5 *A* and *B*). If our mechanism is correct, then propofol should lead to TREK-1 activation. As predicted, propofol, robustly increased TREK-1 currents (Fig. 5*E*) in whole-cell patch clamp. Propofol's effect was significant (Fig. 5*G*, P = 0.017, two-

tailed Student's *t* test) and cotransfection of xPLD2 with TREK-1 completely blocked the propofol-specific current (Fig. 5*F*). Hence, PLD2 activity predicts channel function and this result suggests propofol works through the same pathway as inhaled anesthetics to activate TREK-1, albeit with less potency in C2C12 (*SI Appendix*, Fig. S6 *B* and *C*).

**Anesthetic-Resistant Flies.** If anesthetics disrupt membranes to activate PLD in vivo, then blocking PLD could block or attenuate anesthesia in an animal. Establishing anesthetic sensitivity of PLD in vivo would also establish the membrane and PA signaling as important upstream mediators of anesthetic action independent of a channel. To monitor sedation in vivo, we recorded single-animal measurements (activity and position) of *Drosophila melanogaster* (fruit fly) in a vertically mounted chamber (Fig. 6*A*) (40). Flies are a convenient model since they only have one *pld* gene (41). Flies without functional PLD (PLD$^{null}$) (41) and wild type (WT) (with PLD) were subjected to chloroform vapor and monitored for sedation. Sedation was determined by 5 min of continuous inactivity with a vertical position at the bottom of the fly chamber (Fig. 6*A*).

Sedation of PLD$^{null}$ flies with 2.8 mmol/L chloroform required almost twice the exposure as WT flies (~600 vs. 350 s, P < 0.0001), indicating a highly significant resistance to anesthesia in PLD$^{null}$ (Fig. 6*B*). Almost all flies were anesthetized before the first PLD$^{null}$ fly passed out. The concentration of chloroform is that of the vapor not the concentration in the animal. All flies eventually lost consciousness, suggesting PLD helps set a threshold, but it is not the only pathway controlling anesthetic sensitivity.

**Disruption of GM1 Domains in Whole Brains.** To confirm the presence of GM1 domains in brain tissue, we dissected whole brains from adult flies and labeled them with CTxB and an antibody against the pan-neuronal marker Elav. Confocal imaging (Fig. 6*C*) of CTxB-labeled lipids (GM1, green) showed robust expression of GM1 lipids throughout the fly brain. High concentrations were observed on the membrane of the cell bodies (Fig. 6*C*, zoom) as expected for GM1 lipids. GM1 lipids were also observed in clusters, confirming that lipid organization in the central nervous system (CNS) of flies is similar to our cell culture.

Next, we asked if anesthetic disruption of lipid rafts observed in cell culture also exists in the whole brain of an anesthetized animal. To test this, we anesthetized adult flies with chloroform, dissected their brains, and characterized GM1 lipids in those brains compared with a no-anesthesia control using dSTORM super-resolution imaging (Fig. 6*D*). Consistent with cell culture, the apparent size of GM1 rafts were expanded in fly brains treated with chloroform (Fig. 6*E*). The number of clusters was found to decrease by ~10%.

Lastly, we confirmed that anesthetics activate PLD in neuronal cells of *D. melanogaster*. All anesthetic tested (diethyl ether, chloroform, isoflurane, and propofol) robustly activated *Drosophila* neurons (ML-DmBG2-c2) (Fig. 6 *F–J*). In contrast to N2A and C2C12 cells, propofol induced the greatest activation of PLD, confirming a cell-specific anesthetic sensitivity in a third cell type. FIPI (5-fluoro-2-indolyl des-chlorohalopemide) inhibition (Fig. 6*J*) suggests its mechanism of inhibition is conserved in flies.

**Discussion**

We conclude that the membrane is a target of inhaled anesthetics and that PA and disruption of lipid raft localization contributes to anesthesia in vivo. Our proposed model for TREK-1 in mammalian cells is consistent with most known properties of inhaled anesthetics on the channel (Fig. 2*D*) despite it utilizing an indirect mechanism through PLD2 and lipid
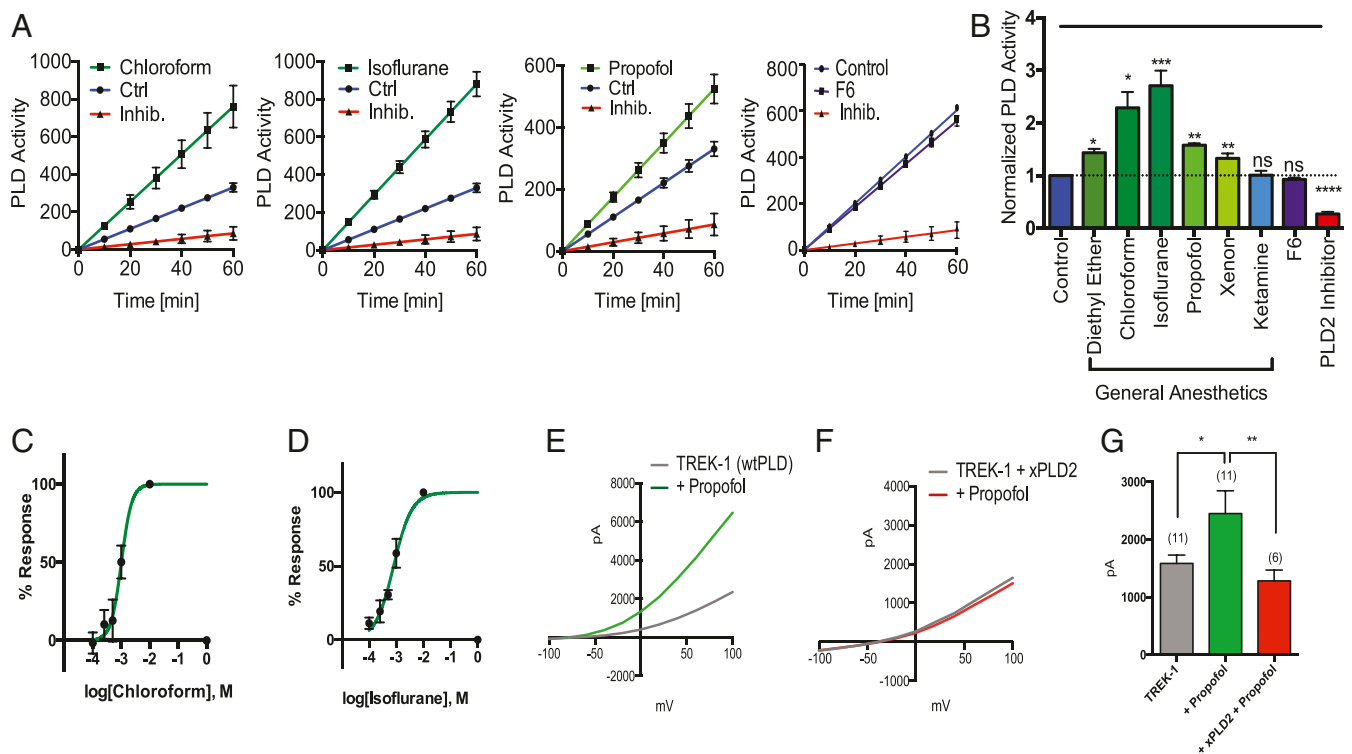
**Fig. 5.** Inhaled anesthetics activates phospholipase D (PLD) through raft disruption. (*A*) Live-cell assays showing the effect of anesthetics on PLD (PLD1 and PLD2) activity in N2A cells. Chloroform (1 mM), isoflurane (1 mM), and propofol (50 μM) increased the PLD activity as compared with the control cells. The nonimmobilizer F6, at predicted Overton–Meyer concentrations, had no effect on the PLD activity and the activity was inhibited by a PLD-specific inhibitor (2.5 to 5 μM) (mean ± SEM, $n = 4$). (*B*) Summary of normalized anesthetic-induced activity of PLD in *A*–*G* at 60 min (mean ± SEM, $n = 4$) (Student's $t$ test results: ns $P > 0.05$; *$P \leq 0.05$; **$P \leq 0.01$; ***$P \leq 0.001$; ****$P \leq 0.0001$). (*C* and *D*) Dose–response of chloroform ($EC_{50} = \sim 1.0$ mM) (*C*) and isoflurane ($EC_{50} = \sim 0.8$ mM) (*D*) on PLD activity through raft disruption. (*E* and *F*) Representative I–V curves showing the effects of propofol on TREK-1 in HEK293 cells using whole-cell patch clamp (*E*), and with xPLD2 (*F*). (*G*) Summary of TREK-1 currents showing an approximately twofold increase when activated by propofol (25 to 50 μM) ($n = 6$) at +40 mV (±SEM) (Student's $t$ test results: *$P < 0.05$; **$P < 0.01$).

binding sites (30, 31, 34). The disruption of PLD2 localization to a lipid nanodomain nicely explains how the C terminus renders a channel anesthetic sensitive when the domain is highly charged, devoid of structure, and has no obvious hydrophobicity expected to bind an anesthetic (37) (*SI Appendix*, Fig. S3 *A* and *B*).

Taken together, the effect of anesthetic treatment and cholesterol depletion establishes two independent functions for cholesterol in GM1 regulation. First, cholesterol regulates the total amount of GM1 rafts, more cholesterol more and larger GM1 rafts (Fig. 1 *A*–*E*). With anesthetics, the amount and size of GM1 rafts is increased. Second, cholesterol increases PLD2 localization to GM1 rafts—anesthetics inhibit this function of cholesterol. Hence, these two functions can be regulated independently. The total amount of GM1 rafts likely helps control the amplitude of a signal and the localization controls the on/off state. PIP$_2$ activates PLD2 by pulling the enzyme out of GM1 rafts (22). By disrupting GM1 localization, anesthetics enhance PIP$_2$ regulation.

Our model relies on the upstream central role of the lipid PA. PA's importance is directly supported by the finding that a single protein that modulates PA production, PLD, dramatically shifted the anesthetic threshold in an animal (Fig. 6*B*). The conclusion is also indirectly supported by the observation of GM1 rafts throughout the brain of flies (Fig. 6*C*), the observed disruption of GM1 rafts in the whole-brain tissue of chloroform-treated flies (Fig. 6*E*), and the modular transfer of anesthetic sensitivity to TRAAK by localization of a PA-producing enzyme (Fig. 3*B*). We expect the lipid to contribute to central regulation of excitability through direct binding to multiple proteins including ion channels (42, 43). Recently, PA emerged as a class of

lipid-regulated ion channel, modulating excitability and pain (28). The role PA-producing enzymes will need to be tested for these channels.

The latency (time delay) of PLD2 mixing in these experiments was dictated by our relatively slow application of anesthetic by gravity flow (*Materials and Methods*). However, theoretical estimates of latency based on distance of PLD2 from its substrate suggest a PLD2-dependent latency of ~650 μs (22), much faster than our application of anesthetic (>10 s). In membranes that are mechanically disrupted, we have measured a PLD2 latency of TREK-1 activation with an upper limit of 2.1 ms (44); we expect disruption by anesthetic is similar. PA can also affect membrane curvature and hydrophobic mismatch, and anesthetics can in theory affect these properties or a PLD1-dependent pathway to regulate TREK-1 (45), but in cultured cells these potential mechanisms, if they contribute, appear to be minor compared to the contribution of PLD2 based on xPLD2 inhibition (Fig. 2 *A*–*C*).

Over the past decade anesthetic research has focused on direct binding of inhaled anesthetics to allosteric sites on proteins (2, 4, 46). Direct binding appears to be incorrect for TREK-1, but our results do not preclude direct binding for other channels. In some instances, the direct binding may be competition of anesthetics with lipid regulatory sites (28) which would be a hybrid protein/lipid mechanism. Contributing to a protein-based narrative, anesthetics are also known to be enantiomer selective (47–49). Interestingly, ordered lipids are also chiral and the ability of an anesthetic to partition into ordered domains will need to be considered in light of the mechanism presented here.
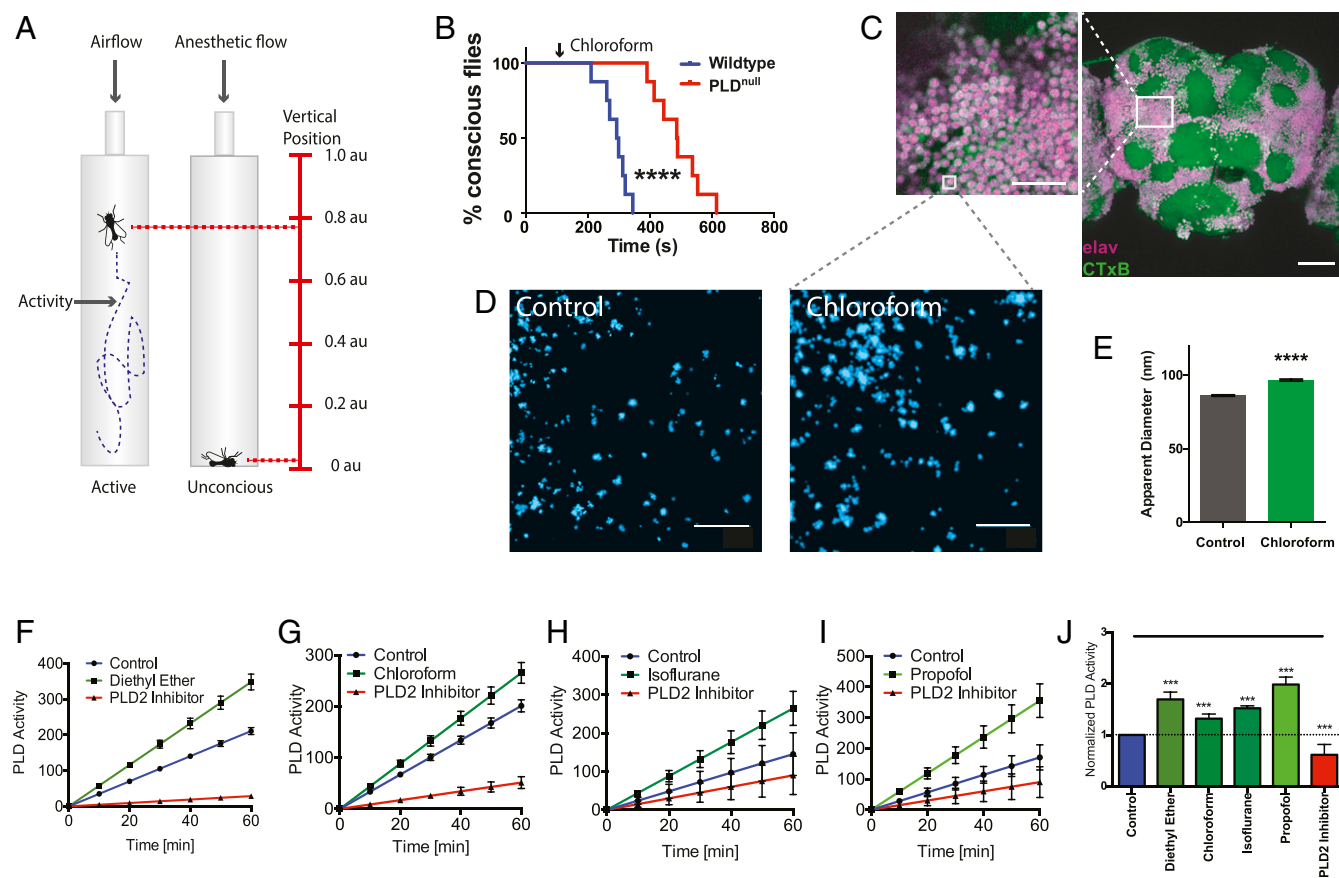
**Fig. 6.** Phospholipase D (PLD) regulates anesthetic sensitivity in *D. melanogaster*. (*A*) Diagram depicting the setup of the anesthetic treatment and the positional recordings of the flies. Fly positions were used to confirm anesthesia. (*B*) Sedation curves showing the percent of unconscious flies over time after chloroform treatment (2.8 mmol/L of air volume) in both WT and PLD$^{null}$ flies. (*C*) Confocal images showing robust labeling of GM1 rafts (CTxB, green) in the membranes of labeled neurons (pan-neuronal Elav antibody, purple) of the whole fly brain. (Scale bar, 500 μm and 25 μm for the zoomed panel.) (*D* and *E*) Flies were treated with chloroform and the GM1 rafts of whole-brain tissue were assayed for anesthetic-induced disruption by super-resolution imaging (dSTORM). (*D*) Super-resolution images with (*Right*) and without (*Left*) sedating chloroform. (*E*) Quantitation of apparent raft size diameter from fixed whole fly brain with and without chloroform. Similar to raft disruption in tissue culture, the GM1 rafts expand in brains of flies treated with chloroform (96.5 ± 0.7 nm vs. 86.0 ± 0.5 nm, respectively). Gray dotted lines indicate a hypothetical zoom compared to the low-resolution imaging of confocal in *C*. (mean ± SEM, $n$ = 16,000 to 17,500, where $n$ is the measurement of an individual raft size). (*F–I*) PLD assays on fly neuronal cells (ML-DmBG2-c2) confirming the activation of PLD by anesthetics: diethyl ether (1 mM) (*F*) chloroform (1 mM) (*G*), isoflurane (1 mM) (*H*), and propofol (50 μM) (*I*). (*J*) Bar graph of normalized activity of PLD in *F–I* at 60 min (mean ± SEM, $n$ = 3 to 4) (Student's *t* test results: ***$P$ < 0.001; ****$P$ < 0.0001).

Many channels are directly palmitoylated (50) and they could be modulated by a change in ion channel localization. For example, the anesthetic channel γ-aminobutyric acid A receptor (GABA$_A$R) gamma subunit is palmitoylated (50) and the alpha subunit was recently shown to bind PIP$_2$ (51). Hence GABA$_A$R is comprised of precisely the same features that render PLD2 anesthetic sensitivity. If and how these features function in GABA$_A$R is not known. Many important signaling molecules are palmitoylated, including tyrosine kinases, GTPases, CD4/8, and almost all G protein alpha subunits (52). Anesthetic disruption of GM1 localization of these proteins likely contributes to the many effects of anesthetics in vivo. The angiotensin converting enzyme 2 (ACE2) receptor for SARS-COV2, that causes COVID19, is also palmitoyated and GM1 disruption may contribute to inhibition of viral entry similar to anesthetics (53, 54).

Direct binding of a lipid mediator may explain why anesthetics typically have the opposite effect on excitatory and inhibitory channels (27, 55). The intermediary, e.g., a signaling lipid, would likely evolve to oppositely regulate excitatory and inhibitory channels. The opposing regulation would combine to systematically increase or decrease nerve cell excitability. In contrast, direct binding of anesthetics to random allosteric sites lacks

obvious rational for the systematic regulation of inhibitory and excitatory channels.

It is unclear why the effectiveness of propofol varied dramatically between cell types. Since GM1 rafts are cholesterol dependent it is tempting to speculate that the amount of cholesterol or the chain length of saturated lipids may affect its efficacy. Alternatively, the difference could be the ability of propofol to partition into the membrane. Due to their hydrophobicity, anesthetics partition, which greatly increases their effective concentration in the cell. Unlike inhaled anesthetics, propofol is typically injected into the blood as an emulsion. The availability of lipid carrier proteins or ability of the cell to directly interact with the emulsion may account for the differences among cell types.

Lastly, we considered the biophysical effect of anesthetics on the bulk membranes or "nonraft" membranes. We saw very little effect of clinical concentration of anesthetics on TREK-1 reconstituted into 1,2-dioleoyl-*sn*-glycero-3-phosphocholine (DOPC) liposomes in our flux assay (*SI Appendix*, Fig. S3 *F* and *G*), a mimic of bulk lipids. This result agrees with previous studies that showed the effect of anesthetics on bulk lipids is insufficient to activate a channel (56) despite the fact that anesthetics fluidize

and thin membranes (7, 57). TREK-1 is very sensitive to membrane thickness (58). It is possible we failed to test an optimal thickness that is responsive in artificial systems; however, the fact that xPLD2 blocked all detectible anesthetic currents in whole cells suggests, in a biological membrane, TREK-1 and PLD2 translocation is the primary mechanism for anesthetic activation of TREK-1, not thinning of bulk lipids.

The mechanism presented here only relies on a nonuniform (heterogeneous) distribution of lipids in the membrane. The mechanism for their distribution should not matter, be it pure lipid partitioning or protein-induced clustering. Nor should the mechanism require that any one raft be long-lived. In fact, given PLD2's equilibrium between GM1 and $PIP_2$ rafts, decreasing the longevity of GM1 rafts is likely a significant in vivo condition that shifts PLD2 to interact more with $PIP_2$. Similarly, transient signaling is speculated in cell growth and differentiation (59).

Our work does not rule out a palmitate-specific binding protein associating with GM1 lipids and clustering of palmitoylated proteins through a specific lipid–protein interaction. While possible, the mechanism is unlikely since mechanical force, anesthetics, and cholesterol depletion share the same pathway for activating TREK-1. It is difficult to rationalize how mechanical force or cholesterol depletion could disrupt an individual lipid from interacting with a protein absent the membrane. Nonetheless the possibility exists and should be investigated.

In conclusion, our data show a pathway where anionic lipids are central mediators of anesthetic action on ion channels and these results suggest lipid regulatory molecules and lipid binding sites in channels may be effective targets for treating nervous system disorders and understanding the thresholds that govern intrinsic nerve cell excitability. Thus, the system we describe here obviously did not evolve to interact with inhaled anesthetics and a search as to what the endogenous analog that activates this physiological system is warranted.

## Materials and Methods

**Sample Preparation for Super-Resolution Microscopy (dSTORM).** Super-resolution microscopy was performed on N2A and C2C12 cells. Confluent cells were first starved overnight with serum-free Dulbecco's Modified Eagle Medium (DMEM) in eight-well chamber slides (Nunc Lab-Tek Chamber Slide System, Thermo Scientific). Cells were then washed and treated with anesthetics or other drugs for 10 min. Chambers containing volatile anesthetic were tightly sealed with aluminum adherent film. Cells were then chemically fixed with 3% paraformaldehyde and 0.1% glutaraldehyde in phosphate buffer saline (PBS) for 10 min at room temperature with shaking, and the fixing solution was quenched by incubating with 0.1% $NaBH_4$ for 7 min followed by three 10-min washes with PBS. Anesthetics or the drugs were maintained in the fixing solution to ensure their effect on the cell. Fixed cells were then permeabilized with 0.2% Triton-X 100 in PBS for 15 min except the cells receiving the CTxB treatment. Cells were blocked using a standard blocking buffer (10% bovine serum albumin [BSA], 0.05% Triton in PBS) for 90 min at room temperature. For labeling, anti-PLD2 antibody (Cell Signaling) with 1:500 dilution and CTxB (Life Technologies) with 1:1,000 dilution in the blocking buffer were simultaneously added to cells and incubated for 60 min at room temperature. Cells were then extensively washed with 1% BSA, 0.05% Triton in PBS five times, 15 min each, before labeling with the secondary antibody diluted into the blocking buffer and incubating for 30 min. Prior to labeling, the secondary antibody was conjugated to either Alexa 647 (to detect CTxB raft) or Cy3B (to detect PLD2). The incubation with secondary antibody was followed by above extensive wash and a single 5-min wash only with PBS. Labeled cells were then postfixed (i.e., fixed a second time) with the previous fixing solution for 10 min without shaking followed by three 5-min washes with PBS and two 3-min washes with deionized distilled water. To elucidate the lipid raft disruption by anesthetics or other drugs, compounds were applied to the reaction buffer at these concentrations: chloroform (1 mM) (Fisher Scientific); isoflurane (1 mM) (Sigma); mβCD (100 μM) (Fisher); diethyl ether (1 mM) (Sigma); ketamine (50 μM) (Cayman Chemicals); and xenon (4.9 mM) (Praxair). Xenon was prepared as a saturated solution. Its concentration was estimated from its solubility in water (0.6 g/L).

**dSTORM Image Acquisition and Analysis.** Imaging was performed with A Zeiss Elyra PS1 microscope using total internal reflection fluorescence (TIRF) mode equipped with an oil-immersion 63× objective. An Andor iXon 897 electron-multiplying CCD camera was used along with the Zen 10D software for image acquisition and processing. The TIRF mode in the dSTORM imaging provided low background high-resolution images of the cell membrane. A total of 10,000 frames with an exposure time of 18 ms were collected for each acquisition. Excitation of the Alexa Fluor 647 dye was achieved using 642-nm lasers and Cy3B was achieved using 561-nm lasers. Cells were imaged in a photo-switching buffer suitable for dSTORM: 1% betamercaptoethanol, 0.4 mg glucose oxidase, and 23.8 μg catalase (oxygen scavengers), 50 mM Tris, 10 mM NaCl, and 10% glucose at pH 8.0. Sample drift during the acquisition was corrected for by an autocorrelative algorithm (60) or tracking several immobile, 100-nm gold fiducial markers or TetraSpec beads using Zen 10D software. The data were filtered to eliminate molecules with localization precisions >50 nm.

Super-resolved images were constructed using the default modules in the Zen software. Each detected event was fitted to a two-dimensional (2D) Gaussian distribution to determine the center of each point spread function (PSF) plus the localization precision. The Zen software also has many rendering options, including the options to remove the localization errors, outliers in brightness and size. The super-resolved images have an arbitrary resolution of 128 pixel/μm. To determine the apparent raft size and the pair correlations, the obtained localization coordinates were converted to be compatible to Vutara SRX software (version 5.21.13) by an Excel macro. Cross-correlation and raft size estimation were calculated through cluster analysis using the default analysis package in the Vutara SRX software (22, 61–63). Cross-correlation function $c(r)$ estimates the spatial scales of coclustering of two signals – the probability of localization of a probe to distance $r$ from another probe (64). Raft sizes are the size of clusters determined by measuring the area of the clusters comprising more than 10 observations.

**In Vivo PLD Activity Measurements.** A nonradioactive method was performed to measure in vivo PLD activity as described previously (22, 37) (*SI Appendix*, Fig. S2). The assay measures the activity of PC hydrolysis which is carried out by both PLD1 and PLD2 isoenzymes. The relative contribution of each cannot be distinguished by our live cell assay. Briefly, N2A, ML-DmBG2-c2, or C2C12 cells were seeded into 96-well flat culture plates with transparent-bottom to reach confluency (~5 × 104 per well). Then the confluent cells were differentiated with serum-free DMEM for a day and washed with 200 μL of PBS. The PLD assay reactions were promptly begun by adding 100 μL of working solution with or without anesthetics or FIPI alone (1 μM), a PLD-specific inhibitor (65). The working solution contained 50 μM Amplex red, 1 U per mL horseradish peroxidase, 0.1 U per mL choline oxidase, and 30 μM dioctanoyl phosphatidylcholine (C8-PC). Anesthetics were directly dissolved into the working buffer from freshly made stocks and incubated overnight before assay reagents were added. In case of volatile anesthetics, 96-well plates were tightly sealed with aluminum adherent films after adding the reaction buffer. The PLD activity and the background (lacking cells) was determined in triplicate for each sample by measuring fluorescence activity with a fluorescence microplate reader (Tecan Infinite 200 PRO, reading from bottom) for 2 h at 37 °C with an excitation wavelength of 530 nm and an emission wavelength of 585 nm. Subsequently, PLD activity was normalized by subtracting the background from the control and treatment activity. Data were then graphed (mean ± SEM) and statistically analyzed (Student's *t* test) with GraphPad Prism 6.

**Electrophysiology.** Whole-cell patch-clamp recordings of TREK-1 currents were made from TREK-1-transfected HEK293T cells as described previously (29). Briefly, HEK293T 50% confluent cells were transiently transfected with 1 μg of DNA (cotransfections of channel with PLD were in a ratio of 1:3, respectively). Voltage ramps (−100 mV to +50 mV) were recorded in the whole-cell configuration. A volatile anesthetic, chloroform, was applied using a gravity-driven (5 mL/min) gas-tight perfusion system. Experimental details are described in *SI Appendix*.

**Channel Purification and Flux Assay.** TREK-1 channel protein purification and flux assay were done as previously described in refs. 35 and 36. Briefly, purified TREK-1 was reconstituted into DOPC/DOPG. Potassium efflux was measured using a pH-sensitive dye coupled with a protonophore m-chlorophenyl hydrazone (CCCP). Experimental details are described in *SI Appendix*.

**SDS/PAGE and Western Blot.** HEK293T cells were transiently transfected; after 48 h of the transfection, cells were lysed in 1.5% n-Dodecyl-β-D-maltoside,

centrifuged separated, blotted, and probed with a rabbit monoclonal antibody against PLD2 (E1Y9G, Cell Signaling). Experimental details are described in *SI Appendix*.

**FRAP.** For FRAP studies, N2A and C2C12 cells were fixed with 3% paraformaldehyde and 0.1% glutaraldehyde for 20 min at 37 °C and labeling with fluorescent CTxB. Recovery was measured out to 5 min after the bleaching step. Experimental details are described in *SI Appendix*.

*Drosophila.*

*General protocols.* Flies were maintained in stocks at 25 °C. For all experiments, male flies were isolated from stocks 1 to 4 d old and allowed to recover in vials of no more than 10 flies for 24 to 48 h before use in protocols.

*Anesthesia in D. melanogaster.* Anesthesia in flies was applied by volatiles and aerosols administered with positional recording (VAAPR) (40) in custom-built narrow-width vertical chambers placed in front of a camera to monitor the fly's positions with or without the chloroform treatment. Wild-type and PLD$^{null}$ flies were gently loaded into the designated chamber using mouth aspiration and the hoses used for compound delivery were attached to the chamber. Flies were allowed to habituate in the chamber while preparing treatment mixtures (~15 min). Mixtures without chloroform contains only water with methylcyclohexanol (MCH) (1: 250), an aversive odor to increase baseline activity of the flies. Chloroform was delivered at known concentrations by calculating the partial pressures of the anesthetic in known dilutions of solvent. Both air control and chloroform air were passed through flow meters to control the overall flow rate of 290 mL/min/chamber. Air was given to all flies for 2 min to record baseline activity/position after which the chloroform was applied to the experimental flies. Activity and position of the flies were tracked using a custom-written program in Python, "opencvArduinoARC_2.0" and data were analyzed by "Noah." Both programs are available in the "flyARC" repository on Github. Time of half maximal anesthesia (T50i) values were obtained using a best-fit variable slope curve; sedation curves were analyzed using the Mantel–Cox test. Curve fitting and statistical tests were determined using GraphPad Prism 6.

*Brain imaging.* Flies were placed into a control vial or a vial containing a chloroform-soaked tissue. Flies were removed, and brains were isolated and placed into buffer containing PBS or PBS + chloroform on ice. After dissections, brains were transferred to a buffer containing PBS with 3% paraformaldehyde and 0.1% glutaraldehyde and allowed to fix while rocking overnight at 4 °C. The following day the tissue was rinsed with PBS containing 0.5% Triton X-100 and 0.5% BSA. This buffer was used for all

additional steps unless otherwise stated. Tissue was rinsed 2× for 1 h after which buffer with additional 30 mg of BSA was added and allowed to rock at room temperature for 1.5 h. Buffer was removed and identical buffer containing primary antibodies (Developmental Studies Hybridoma Bank, Rat-Elav-7E8A10, 1:200) was added to the tissue after which it was rocked for 3 h at room temperature and then overnight at 4 °C. The following day buffer was used to rinse the tissue as was done previously. Secondary antibody (Jackson ImmunoResearch, 112-606-072; 1:500) was then applied in a similar manner as before but rocking at 4 °C was extended to 5 d. On the fifth day, the tissue was rinsed once again 2× and then in PBS alone. Tissue was then prepared for imaging. CTxB (1:500) was treated as a secondary antibody. Super-resolution imaging was performed as described above. For whole-brain imaging confocal imaging was used after mounting the tissue onto a coverslip using standard protocols.

**Statistical Analyses.** All of the data calculations and plots were performed using Prism6 (GraphPad software) or Microsoft Excel. Biochemical experiments were done three to four times to ensure reproducibility. To ensure reproducible effect sizes, super-resolution imaging was carried out at least two times on multiple cells. To obtain a precise measurement of apparent raft size, >1,000 raft particles were imaged, and a mean was taken for all of the observed rafts. All of the microscopy was performed in random order to avoid any experimental bias. Statistical significance was evaluated using ANOVA with post hoc Dunnett's test, two-tailed $t$ tests, parametric or nonparametric, wherever appropriate. Data are presented as the mean and the error bars with SD or 95% confidence interval as appropriate. Significance is indicated by *$P \leq 0.05$, **$P \leq 0.01$, ***$P \leq 0.001$, and ****$P \leq 0.0001$.

**Data Availability.** Data for super-resolution imaging, electrophysiology, and PLD enzyme activity are available at https://data.mendeley.com/ (66).

1. J. A. Campagna, K. W. Miller, S. A. Forman, Mechanisms of actions of inhaled anesthetics. *N. Engl. J. Med.* **348**, 2110–2124 (2003).
2. B. W. Urban, M. Bleckwenn, M. Barann, Interactions of anesthetics with their targets: Non-specific, specific or both? *Pharmacol. Ther.* **111**, 729–770 (2006).
3. A. Kopp Lugli, C. S. Yost, C. H. Kindler, Anaesthetic mechanisms: Update on the challenge of unravelling the mystery of anaesthesia. *Eur. J. Anaesthesiol.* **26**, 807–820 (2009).
4. N. P. Franks, General anaesthesia: From molecular targets to neuronal pathways of sleep and arousal. *Nat. Rev. Neurosci.* **9**, 370–386 (2008).
5. J. M. Sonner, A hypothesis on the origin and evolution of the response to inhaled anesthetics. *Anesth. Analg.* **107**, 849–854 (2008).
6. J. M. Sonner, R. S. Cantor, Molecular mechanisms of drug action: An emerging view. *Annu. Rev. Biophys.* **42**, 143–167 (2013).
7. M. Weinrich, D. L. Worcester, The actions of volatile anesthetics: A new perspective. *Acta Crystallogr. D Struct. Biol.* **74**, 1169–1177 (2018).
8. D. Lingwood, K. Simons, Lipid rafts as a membrane-organizing principle. *Science* **327**, 46–50 (2010).
9. E. Sezgin, I. Levental, S. Mayor, C. Eggeling, The mystery of membrane organization: Composition, regulation and roles of lipid rafts. *Nat. Rev. Mol. Cell Biol.* **18**, 361–374 (2017).
10. I. Levental, M. Grzybek, K. Simons, Raft domains of variable properties and compositions in plasma membrane vesicles. *Proc. Natl. Acad. Sci. U.S.A.* **108**, 11411–11416 (2011).
11. S. A. Jones, S. H. Shim, J. He, X. Zhuang, Fast, three-dimensional super-resolution imaging of live cells. *Nat. Methods* **8**, 499–508 (2011).
12. B. Huang, W. Wang, M. Bates, X. Zhuang, Three-dimensional super-resolution imaging by stochastic optical reconstruction microscopy. *Science* **319**, 810–813 (2008).
13. E. Betzig et al., Imaging intracellular fluorescent proteins at nanometer resolution. *Science* **313**, 1642–1645 (2006).
14. S. T. Hess, T. P. K. K. Girirajan, M. D. Mason, Ultra-high resolution imaging by fluorescence photoactivation localization microscopy. *Biophys. J.* **91**, 4258–4272 (2006).
15. H. I. Ingólfsson et al., Computational lipidomics of the neuronal plasma membrane. *Biophys. J.* **113**, 2271–2280 (2017).
16. S. Moon et al., Spectrally resolved, functional super-resolution microscopy reveals nanoscale compositional heterogeneity in live-cell membranes. *J. Am. Chem. Soc.* **139**, 10944–10947 (2017).
17. R. A. Lerner, A hypothesis about the endogenous analogue of general anesthesia. *Proc. Natl. Acad. Sci. U.S.A.* **94**, 13375–13377 (1997).
18. E. Gray, J. Karslake, B. B. Machta, S. L. Veatch, Liquid general anesthetics lower critical temperatures in plasma membrane vesicles. *Biophys. J.* **105**, 2751–2759 (2013).
19. D. Papahadjopoulos, K. Jacobson, G. Poste, G. Shepherd, Effects of local anesthetics on membrane properties. I. Changes in the fluidity of phospholipid bilayers. *Biochim. Biophys. Acta* **394**, 504–519 (1975).
20. A. G. Lee, Model for action of local anaesthetics. *Nature* **262**, 545–548 (1976).
21. C. Dart, Lipid microdomains and the regulation of ion channel function. *J. Physiol.* **588**, 3169–3178 (2010).
22. E. N. Petersen, H.-W. Chung, A. Nayebosadri, S. B. Hansen, Kinetic disruption of lipid rafts is a mechanosensor for phospholipase D. *Nat. Commun.* **7**, 13873 (2016).
23. M. McDermott, M. J. O. Wakelam, A. J. Morris, Phospholipase D. *Biochem. Cell Biol.* **82**, 225–253 (2004).
24. I. Levental, D. Lingwood, M. Grzybek, U. Coskun, K. Simons, Palmitoylation regulates raft affinity for the majority of integral raft proteins. *Proc. Natl. Acad. Sci. U.S.A.* **107**, 22050–22054 (2010).
25. G. van den Bogaart et al., Membrane protein sequestering by ionic protein-lipid interactions. *Nature* **479**, 552–555 (2011).
26. J. Wang, D. A. Richards, Segregation of PIP2 and PIP3 into distinct nanoscale regions within the plasma membrane. *Biol. Open* **1**, 857–862 (2012).
27. E. N. Petersen, M. A. Pavel, H. Wang, S. B. Hansen, Disruption of palmitate-mediated localization; a shared pathway of force and anesthetic activation of TREK-1 channels. *Biochim. Biophys. Acta Biomembr.* **1862**, 183091 (2020).
28. C. V. Robinson, T. Rohacs, S. B. Hansen, Tools for understanding nanoscale lipid regulation of ion channels. *Trends Biochem. Sci.* **44**, 795–806 (2019).
29. Y. Comoglio et al., Phospholipase D2 specifically regulates TREK potassium channels via direct interaction and local production of phosphatidic acid. *Proc. Natl. Acad. Sci. U.S.A.* **111**, 13547–13552 (2014).
30. A. J. Patel et al., Inhalational anesthetics activate two-pore-domain background K+ channels. *Nat. Neurosci.* **2**, 422–426 (1999).
31. M. Gruss et al., Two-pore-domain K+ channels are a novel target for the anesthetic gases xenon, nitrous oxide, and cyclopropane. *Mol. Pharmacol.* **65**, 443–452 (2004).

32. C. Heurteaux et al., TREK-1, a K+ channel involved in neuroprotection and general anesthesia. EMBO J. **23**, 2684–2695 (2004).

33. T. C. Sung et al., Mutagenesis of phospholipase D defines a superfamily including a trans-Golgi viral protein required for poxvirus pathogenicity. EMBO J. **16**, 4519–4530 (1997).

34. E. J. Bertaccini, R. Dickinson, J. R. Trudell, N. P. Franks, Molecular modeling of a tandem two pore domain potassium channel reveals a putative binding site for general anesthetics. ACS Chem. Neurosci. **5**, 1246–1252 (2014).

35. Z. Su, E. C. Brown, W. Wang, R. MacKinnon, Novel cell-free high-throughput screening method for pharmacological tools targeting K+ channels. Proc. Natl. Acad. Sci. U. S. A. **113**, 5748–5753 (2016).

36. C. Cabanos, M. Wang, X. Han, S. B. Hansen, A soluble fluorescent binding assay reveals PIP$_2$ antagonism of TREK-1 channels. Cell Rep. **20**, 1287–1294 (2017).

37. M. A. M. A. Pavel, H. W. Chung, E. N. N. Petersen, S. B. S. B. Hansen, Polymodal mechanism for TWIK-related K+ channel inhibition by local anesthetic. Anesth. Analg. **129**, 973–982 (2019).

38. S. G. Brohawn, E. B. Campbell, R. MacKinnon, Physical mechanism for gating and mechanosensitivity of the human TRAAK K+ channel. Nature **516**, 126–130 (2014).

39. J. F. MacDonald et al., Actions of ketamine, phencyclidine and MK-801 on NMDA receptor currents in cultured mouse hippocampal neurones. J. Physiol. **432**, 483–508 (1991).

40. E. N. Petersen, K. R. Clowes, S. B. Hansen, Measuring anesthetic resistance in Drosophila by VAAPR. bioRxiv:10.1101/797209 (10 October 2019).

41. R. Thakur et al., Phospholipase D activity couples plasma membrane endocytosis with retromer dependent recycling. eLife **5**, 1–23 (2016).

42. S. B. Hansen, X. Tao, R. MacKinnon, Structural basis of PIP2 activation of the classical inward rectifier K+ channel Kir2.2. Nature **477**, 495–498 (2011).

43. S. B. Hansen, Lipid agonism: The PIP2 paradigm of ligand-gated ion channels. Biochim. Biophys. Acta **1851**, 620–628 (2015).

44. E. N. Petersen, et al., Phospholipase D transduces force to TREK-1 channels in a biological membrane. bioRxiv:10.1101/758896 (5 September 2019).

45. R. S. Cantor, The lateral pressure profile in membranes: A physical mechanism of general anesthesia. Biochemistry **36**, 2339–2344 (1997).

46. H. C. Hemmings, Jr et al., Emerging molecular mechanisms of general anesthetic action. Trends Pharmacol. Sci. **26**, 503–510 (2005).

47. E. I. Eger, 2nd et al., Minimum alveolar anesthetic concentration values for the enantiomers of isoflurane differ minimally. Anesth. Analg. **85**, 188–192 (1997).

48. R. Dickinson, I. White, W. R. Lieb, N. P. Franks, Stereoselective loss of righting reflex in rats by isoflurane. Anesthesiology **93**, 837–843 (2000).

49. D. F. Covey et al., Enantioselectivity of pregnanolone-induced gamma-aminobutyric acid(A) receptor modulation and anesthesia. J. Pharmacol. Exp. Ther. **293**, 1009–1016 (2000).

50. M. J. Shipston, Ion channel regulation by protein palmitoylation. J. Biol. Chem. **286**, 8709–8716 (2011).

51. D. Laverty et al., Cryo-EM structure of the human α1β3γ2 GABA$_A$ receptor in a lipid bilayer. Nature **565**, 516–520 (2019).

52. C. Aicart-Ramos, R. A. Valero, I. Rodriguez-Crespo, Protein palmitoylation and subcellular trafficking. Biochim. Biophys. Acta **1808**, 2981–2994 (2011).

53. G. M. Li, Y. G. Li, M. Yamate, S. M. Li, K. Ikuta, Lipid rafts play an important role in the early stage of severe acute respiratory syndrome-coronavirus life cycle. Microbes Infect. **9**, 96–102 (2007).

54. Y. Lu, D. X. Liu, J. P. Tam, Lipid rafts are involved in SARS-CoV entry into Vero E6 cells. Biochem. Biophys. Res. Commun. **369**, 344–349 (2008).

55. M. D. Krasowski, N. L. Harrison, General anaesthetic actions on ligand-gated ion channels. Cell. Mol. Life Sci. **55**, 1278–1303 (1999).

56. K. F. Herold, R. L. Sanford, W. Lee, O. S. Andersen, H. C. Hemmings, Jr, Clinical concentrations of chemically diverse general anesthetics minimally affect lipid bilayer properties. Proc. Natl. Acad. Sci. U.S.A. **114**, 3109–3114 (2017).

57. R. D. Booker, A. K. Sum, Biophysical changes induced by xenon on phospholipid bilayers. Biochim. Biophys. Acta **1828**, 1347–1356 (2013).

58. A. Nayebosadri, E. N. Petersen, C. Cabanos, S. B. Hansen, A membrane thickness sensor in TREK-1 channels transduces mechanical force. SSRN Electron. J. bioRxiv: 10.2139/ssrn.3155650 (8 April 2018).

59. A. S. Harding, J. F. Hancock, Using plasma membrane nanoclusters to build better signaling circuits. Trends Cell Biol. **18**, 364–371 (2008).

60. M. J. Mlodzianoski et al., Sample drift correction in 3D fluorescence photoactivation localization microscopy. Opt. Express **19**, 15009–15019 (2011).

61. M. A. Kiskowski, J. F. Hancock, A. K. Kenworthy, On the use of Ripley's K-function and its derivatives to analyze domain size. Biophys. J. **97**, 1095–1103 (2009).

62. P. Sengupta, T. Jovanovic-Talisman, J. Lippincott-Schwartz, Quantifying spatial organization in point-localization superresolution images using pair correlation analysis. Nat. Protoc. **8**, 345–354 (2013).

63. J. M. Hartley et al., Super-resolution imaging and quantitative analysis of membrane protein/lipid raft clustering mediated by cell-surface self-assembly of hybrid nanoconjugates. ChemBioChem **16**, 1725–1729 (2015).

64. P. Sengupta et al., Probing protein heterogeneity in the plasma membrane using PALM and pair correlation analysis. Nat. Methods **8**, 969–975 (2011).

65. W. Su et al., 5-Fluoro-2-indolyl des-chlorohalopemide (FIPI), a phospholipase D pharmacological inhibitor that alters cell spreading and inhibits chemotaxis. Mol. Pharmacol. **75**, 437–446 (2009).

66. M. A. Pavel, Studies on the mechanism of general anesthesia. Mendeley Data. http://dx.doi.org/10.17632/rgsgbbyrws. Deposited 16 May 2020.